

LBL-27248, Book Chapter in Large Area Chromogenics: Materials and Devices for Transmittance Control, C.M. Lampert and C.G. Granqvist, Optical Engineering Press, Bellingham, WA, 1989.

Chemical and Optical Studies of Electrochromic Hydrated Nickel Oxide Films and Devices

Carl M. Lampert

Lawrence Berkeley Laboratory, Applied Science Division,
University of California, Berkeley, CA 94720 USA*

June 1989

*This work was supported by the Assistant Secretary for Conservation and Renewable Energy, Office of Solar Heat Technologies, Solar Buildings Division of the U.S. Department of Energy under Contract No. DE-AC03-76SF00098.

Chemical and Optical Studies of Electrochromic Hydrated Nickel Oxide Films and Devices

Carl M. Lampert

Lawrence Berkeley Laboratory, Applied Science Division,
University of California, Berkeley, CA 94720, USA

1. INTRODUCTION

Over the last few years, hydrated nickel oxide or hydroxide has gained interest as an electrochromic material¹. It has many important features. First it shows a transparent to bronze coloration which is suitable for a number of architectural, vehicle and aerospace glazing applications. This material is stable in an alkaline environment and colors and bleaches at potentials below 1.0V and below the oxygen and hydrogen evolution potentials. It can be deposited by a wide range of processes, including anodic and cathodic electrodeposition, r.f. and d.c. sputtering, vacuum evaporation, chemical vapor deposition, and sol-gel processes. In this work we will discuss films made chiefly by anodic electrodeposition. Some of the best characteristics are seen in films made by electrodeposition. The properties of films made by other deposition processes will be discussed in subsequent chapters. Much of the electrochemical knowledge about hydrated nickel oxide comes from studies of metallic nickel electrodes used in batteries. The study of hydrated nickel oxide based electrochromic devices is just emerging, and so far very few devices have been reported²⁻⁴. Some of the work by my group on nickel based devices will be outlined later in this chapter.

There are several challenges related to electrochromic hydrated nickel oxide. First, the electrochromic reaction for hydrated nickel oxide should be resolved. Only very simplified reactions have been reported. The significant coloration ions should be verified. So far, there is experimental evidence that the proton is responsible for coloration. However there is further evidence that hydroxyl ion is important in the hydroxide to oxyhydroxide reaction. There still remains the question whether other ions such as lithium in an aprotic environment will color nickel oxide effectively and reversibly. In a subsequent chapter⁵, data will be reported on the effect of doping hydrated nickel oxide with a variety of ions, and how ions such as cerium, lanthanum, lithium and yttrium can be beneficial to durability. Overall, the amorphous and crystalline structure of the different types of electrochromic hydrated nickel oxide need to be better characterized. The surface morphology and porosity should also be studied because of their strong influence on coloration intensity and switching rate. A summary of the current state-of-the-art will be presented here.

An electrochromic hydrated nickel oxide device can be fabricated by three methods: (1) a laminated device consisting of an active electrode and ion storage electrode laminated together by a polymer ion conductor or polyelectrolyte, (2) a solid state device made up of sequentially deposited layers, (3) a dispersed electrochromic in a solid or semi-solid electrolyte. A schematic example of the laminated hydrated nickel oxide device is illustrated in Fig. 1. Also, the tin oxide layer shown in this figure could be another conductive oxide such as $\text{In}_2\text{O}_3:\text{Sn}$ or $\text{ZnO}:\text{Al}$.

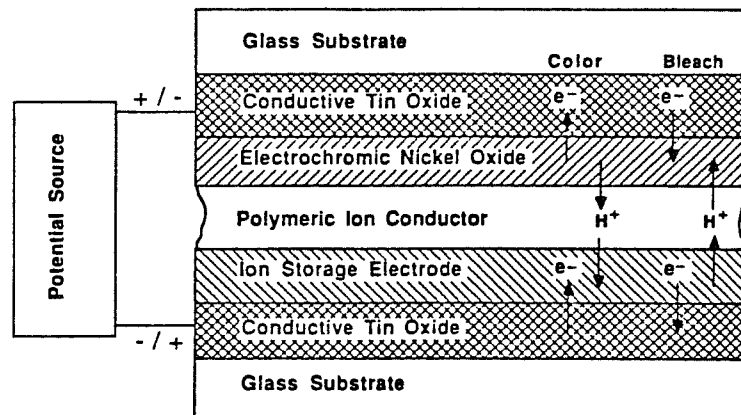


Fig. 1. Generalized schematic of a laminated hydrated nickel oxide electrochromic device (not to scale). Depicted is ionic and electronic flow during coloration and bleaching.

To produce a practical hydrated nickel oxide electrochromic device, both ion conductors and ion storage electrodes have to be fabricated. Currently, there is considerable effort to develop suitable layers for tungsten oxide devices based on protic acid and lithium aprotic electrolytes. Ion storage layers and electrolytes developed for tungsten oxide devices are not necessarily chemically compatible with the hydrated nickel oxide. The search for materials compatible with the alkaline environment of hydrated nickel oxide has begun recently. As a result of this work, I expect to see a variety of hydrated nickel oxide based devices developed in the future. Much of the following work comes from our own studies on hydrated nickel oxide. Further detail can be gained from our published work^{4, 6-8}.

2. PREPARATION OF FILMS

To make working electrodes, hydrated nickel oxide is deposited onto fluorine doped tin oxide ($\text{SnO}_2\text{:F}$) coated glass substrates. The tin oxide layer serves as a transparent electrical conductor. The substrates used in this investigation were 3 mm thick, which is thicker than glass normally used for lamination (1.5-2 mm). The tin oxide coating was supplied by the Watkins-Johnson Company (Scotts Valley, CA, USA). It was made by chemical vapor deposition. Tin doped indium oxide has also been used as a transparent conductor with some of our films. The tin oxide coating had a sheet resistance of 5-25 ohm/sq. To make good electrical contact, a wire was attached to the conductive coating with silver epoxy.

The electrochemical working solution used to deposit the hydrated nickel oxide consisted of a mixture of 0.1M $\text{NiSO}_4 \cdot 6\text{H}_2\text{O}$ and 0.1M NH_4OH at 23°C. The solution was magnetically stirred for 5-10 min. A platinum electrode served as the counter-electrode. A Scanning Potentiostat (Princeton Applied Research, Model 173), was used to deposit the coatings anodically. A triangular potential from -500 mV to +1500 mV versus SCE (Standard Calomel Electrode) was applied between the tin oxide coated electrode and the counter-electrode. The sweep rate was 20mV/s. A hydrated nickel oxide film of approximately 120 nm formed after five cycles. Thickness was determined by scanning profilometry for several samples. In these

studies films of approximately 12, 50 and 120 nm thick were used. Upon formation of the film, the electrode was removed and rinsed in distilled water.

Other deposition solution compositions were experimented with before the former bath was developed. A solution consisting of 0.1M $\text{NiSO}_4 \cdot 6\text{H}_2\text{O}$, 0.1M $\text{C}_2\text{H}_3\text{NaO}_2$, and 0.001M KOH under the same operating conditions made acceptable films but provided less uniformity in the deposit. The nitrate solution used in cathodic deposition was also experimented with. It consisted of 0.45M $\text{Ni}(\text{NO}_3)_2 \cdot 6\text{H}_2\text{O}$, and 1.75M NaOH. Films produced from this bath gave good uniformity but less cyclic stability than the sulfate baths in our studies. Variations of the nitrate deposition process have been used by other investigators⁵.

3. CYCLIC VOLTAMMETRY

Cyclic voltammetry was performed on freshly made hydrated nickel oxide electrodes. The optical switching characteristics were then studied by cycling the electrode with the potentiostat⁶. A range of electrolyte concentrations, 1-0.001M KOH, LiOH, or KCL were used in these experiments. Depending upon the exact conditions of deposition, the electrode could remain out of solution in its colored state for several hours before fading. The experimental arrangement for voltammetry is shown schematically in Fig. 2.

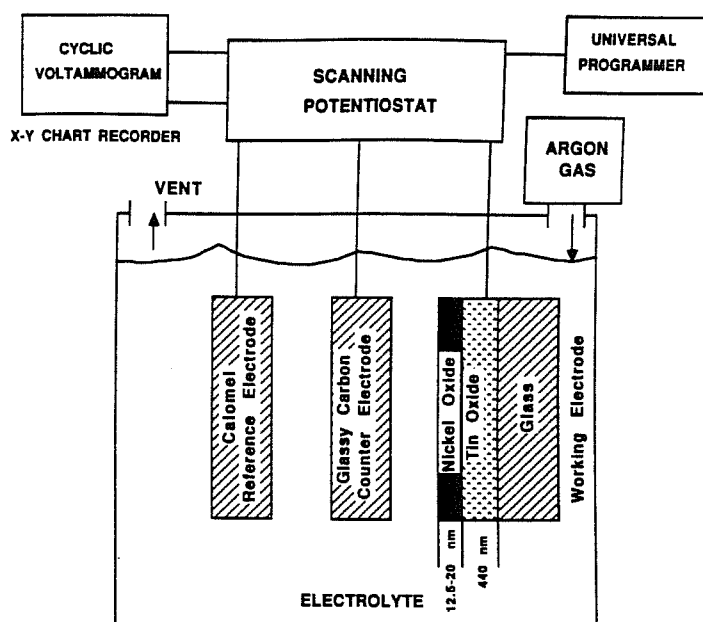


Fig. 2. Schematic of a liquid cell arrangement for voltammetry and electrochemical studies.

An investigation was made using a periodically increasing triangular potential during the anodic half-cycle. The electrolyte was 1.0M KOH with a sweep rate of 50 mV/s. The starting potential was -500 mV in all cases. For the first cycle the anodic limit was +300 mV, and on each subsequent cycle it was increased 100 mV, ultimately limited to +750 mV. After eight cycles, the electrode was allowed to cycle between -500 mV and +750 mV, to a total of fifty cycles. However, after the sixth cycle (600 mV anodic potential), no further change was noted. The data in Fig. 3 show a predominant anodic peak at 390 mV

(SCE) and a single predominant cathodic peak at 190 mV (SCE). Also, an oxygen-evolution peak occurs at about 550 mV (SCE). Similar results have been noted by other investigators⁹⁻¹² The electrode response is similar to that noted for our study of oxidized metallic nickel electrodes⁶.

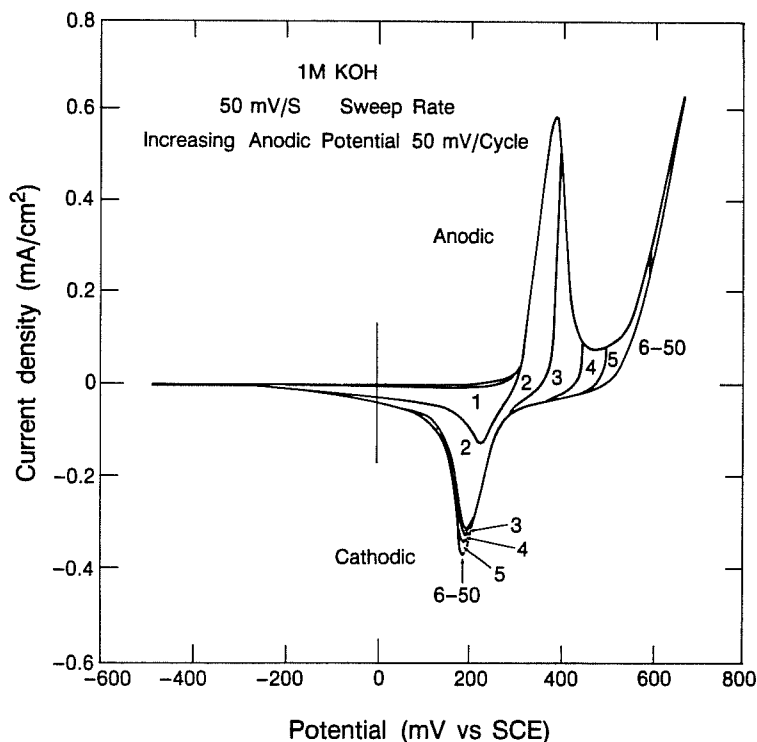


Fig. 3. Increasing anodic potential cyclic voltammogram of a hydrated nickel oxide/SnO₂:F/glass electrode in 1.0M KOH at a sweep rate of 50mV/s. The anodic potential starts with 300 mV, stepping 100 mV per cycle to 750 mV. The numbers on the figure indicate the cycle number.

The oxidation reaction taking place at the anodic peak is identified as (in simplified form, using the proton as the active ion)^{9,11,13-15}:



At the cathodic peak the reduction reaction is determined to be:



In Fig. 3, it should be noted that during the third to sixth cycle, there is a slight increase in the cathodic peak current. This increase during the first few cycles indicates that NiOOH is not completely reduced to Ni(OH)₂. The cathodic peak potential did not change during these early cycles, indicating stability of the

film even though the oxygen-evolution potential had been exceeded. Reactions [1] and [2] can be written with the hydroxyl ion as the active ion too. The distinct phases noted by other investigators for the alpha and beta forms of $\text{Ni}(\text{OH})_2$ and the alpha and beta forms of NiOOH were not noted here¹³⁻¹⁵. A further discussion of the coloration reaction in the film is in section 4.5.

Potential-scan experiments were carried out with sweep rates of 5-150 mV/s in 1.0M KOH electrolyte. From these experiments, proton diffusion information for the reaction can be obtained. The results of the potential scan are shown in Fig. 4.

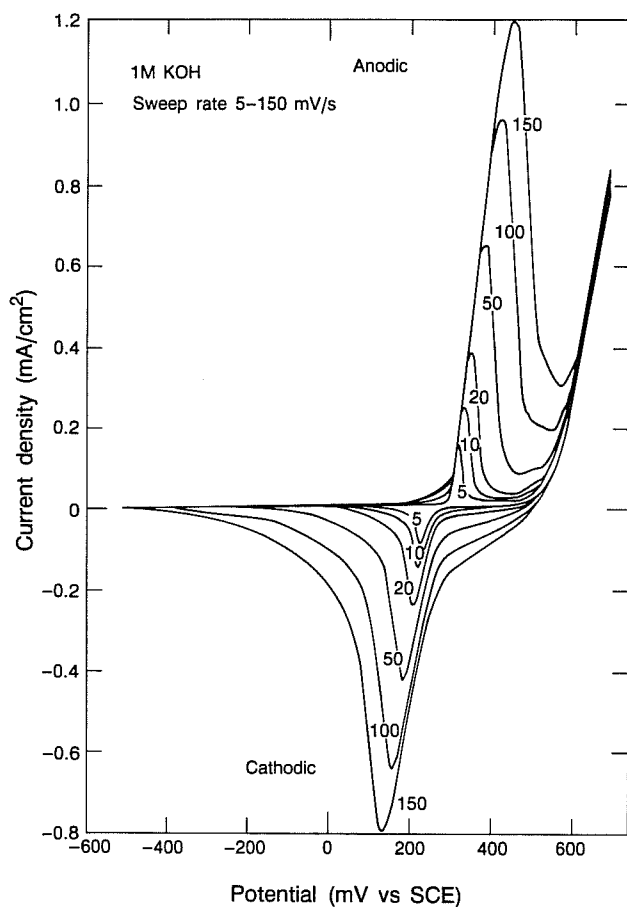


Fig. 4. Potential-scan experiment showing voltammetry of a hydrated nickel oxide/ $\text{SnO}_2\text{:F}$ /glass electrode in 1.0M KOH. The sweep rates are given in mV/s in the figure. The numbers on the figure indicate the cycle number.

By plotting the peak current density versus the square root of the sweep rate, as shown in Figs. 5 and 6, a linear relationship is found, which implies that the reaction is purely diffusion controlled. Also, impedance spectroscopy has indicated diffusion controlled behavior during coloring and bleaching¹⁶. To determine if the diffusion of the proton was controlling the reaction, the concentration of hydroxyl ions was varied from 1.0M to 0.001M with KOH. A supporting electrolyte of KCL was used to keep the electrolyte conductivity constant. The anodic peak currents for these different electrolyte concentrations are shown in Fig. 5. From these data, it is noted that the slopes of the curves, which are a function of the diffusion coefficient of a single ion species, do not depend on the hydroxyl ion concentration (at least for this range

of electrolyte concentrations). Therefore, the proton must be the significant ion in the rate-determining process for both the anodic and cathodic cycles, at least in the electrolyte concentration range studied. Other researchers have identified this ion as a proton too^{9-11,13,15}. Another way to separate the role protons and hydroxyl ions play in coloration would be to overcoat the nickel oxide electrode with ion selective membrane and repeat the voltammetry experiments.

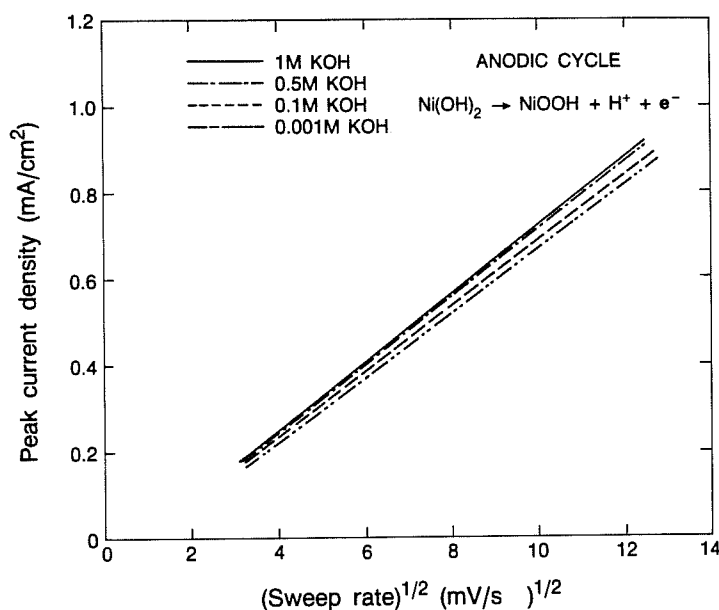


Fig. 5. Anodic peak current density versus (sweep rate)^{0.5} for the coloration of a hydrated nickel oxide/SnO₂:F/glass electrode in 0.001M to 1.0M KOH.

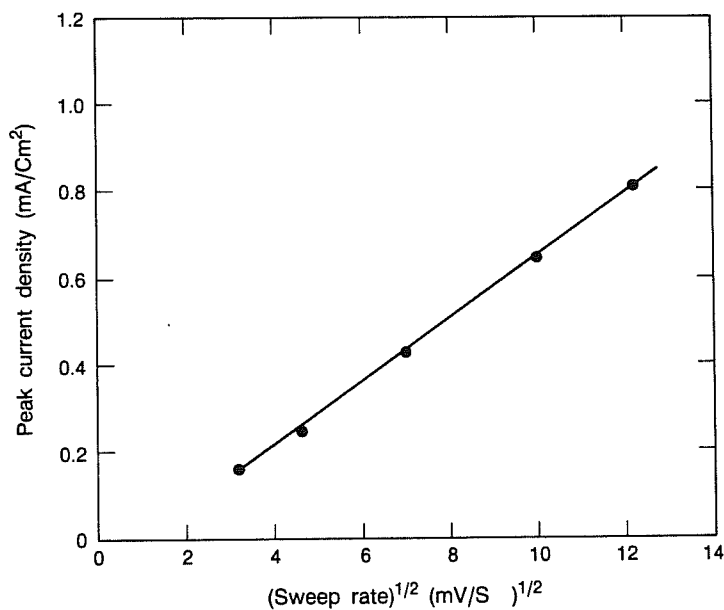


Fig. 6. Cathodic peak current density versus (sweep rate)^{0.5} for the bleaching of a hydrated nickel oxide/SnO₂:F/glass electrode in 1.0M KOH.

The maximum proton-diffusion coefficient for thick hydrated nickel oxide films (1-1.8 μm) has been determined by semi-infinite and finite diffusion models^{15,17}. For those films, the diffusion coefficient was estimated to be in the range of 10^{-10} to 10^{-11} cm^2/s with a diffusion length of 0.55 μm . The films used in here may be too thin to be applicable to these diffusion models.

Variable electrolyte-concentration experiments using a constant sweep rate were conducted to determine if a very low concentration of hydroxyl ions influences the proton-reaction mechanism. The range of electrolyte concentrations was 0.0001M to 1.0M KOH, with KCl added to keep conductivity constant. A sweep rate of 50 mV/s was used. The results are shown in Figs. 7 and 8.

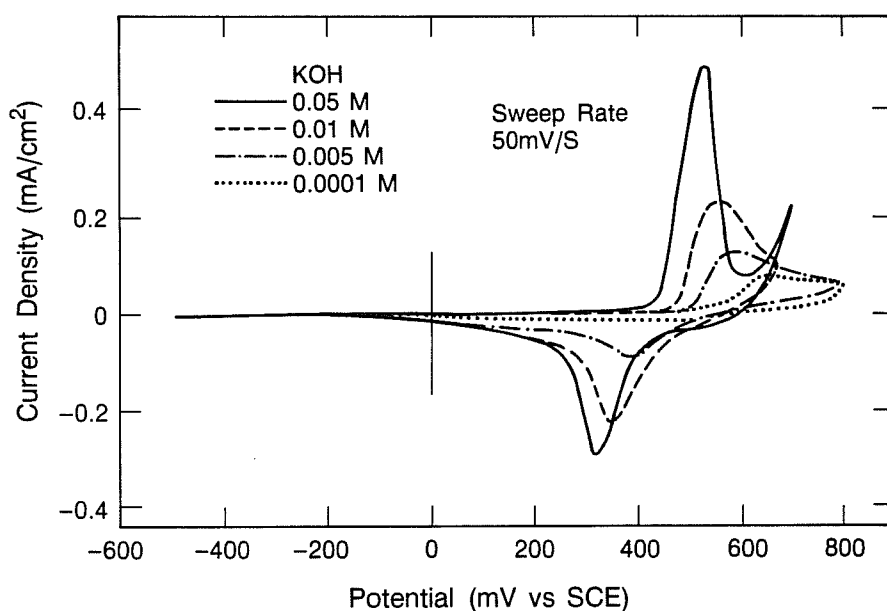


Fig. 7. Cyclic voltammetry of a hydrated nickel oxide/SnO₂:F/glass electrode in 0.0001-0.05M KOH, at a sweep rate of 50 mV/s.

There is an overall trend of anodic and cathodic peak shifting to higher potentials for lower concentrations, resulting in higher reversible potentials ranging from 2.4-5.22 V (SCE) (Ref 7). This shift has been noted in KOH and other alkaline electrolytes by other investigators^{15,18}. This result demonstrates that the concentration of surface hydroxyl groups has a significant impact on the movement of protons diffusing within the films to the film-electrolyte interface. Also, this experiment shows that generally the concentration of hydroxyl ions has no significant role in the anodic oxidation of hydrated nickel oxide, suggesting that the diffusion of the proton is the rate-limiting process.

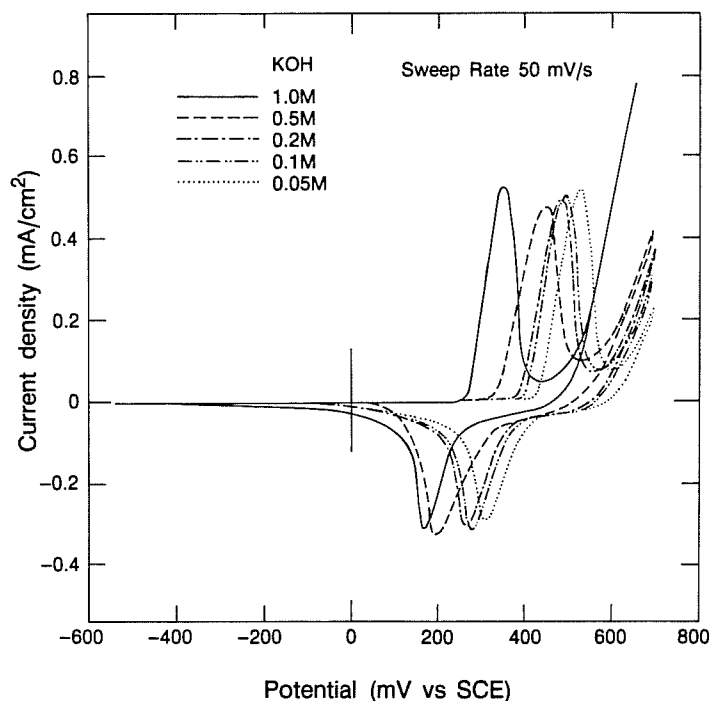


Fig. 8. Cyclic voltammetry of a hydrated nickel oxide/SnO₂:F/glass electrode in 0.05-1.0M KOH, at a sweep rate of 50 mV/s .

To further understand the role of surface hydroxyl groups, we compared the electrochemical switching of hydrated nickel oxide films as they were alternated between neutral and highly alkaline electrolytes. The beginning experiment used a 1.0M KCl electrolyte which gave no voltammetric response. When the film was transferred and cycled in 1.0M KOH the oxidation and reduction peaks shown in Fig. 9A appeared. The film was next removed at a potential above the coloration peak and transferred to 1.0M KCl; a reduction peak was seen only for the first cycle, as shown in Fig. 9B. This demonstrates that the hydroxyl ions must be present at the film surface for oxidation to occur. In another experiment, the film electrode was removed from 1.0M KOH in the bleached state and transferred to 1.0M KCl where 1.0M HCl was also added. During cycling, no anodic or cathodic peaks were observed, as noted in Fig. 9C. The film was then cycled in 1.0M KOH and again showed the oxidation/reduction peaks (Fig. 9D) This experiment indicates that oxidation cannot occur in the absence of hydroxyl ions.

Lithium ions were intercalated into the hydrated nickel oxide to increase its stability to oxygen evolution during coloration⁴. The addition of lithium ions alters the chemical binding and electrostatic forces in the layered lattice of hydrated nickel oxide. The Li⁺ ions in the hydrated nickel oxide crystal lattice prevent the incorporation of K⁺ ions. The net effect is to increase the oxygen overvoltage by hindering the recombination of adsorbed oxygen¹⁹. Also, it has been shown that lithium helps to tightly bind water in the interlayer structure of hydrated nickel oxide²⁰. These factors provide the hydrated nickel oxide electrode with greater charge capacity.

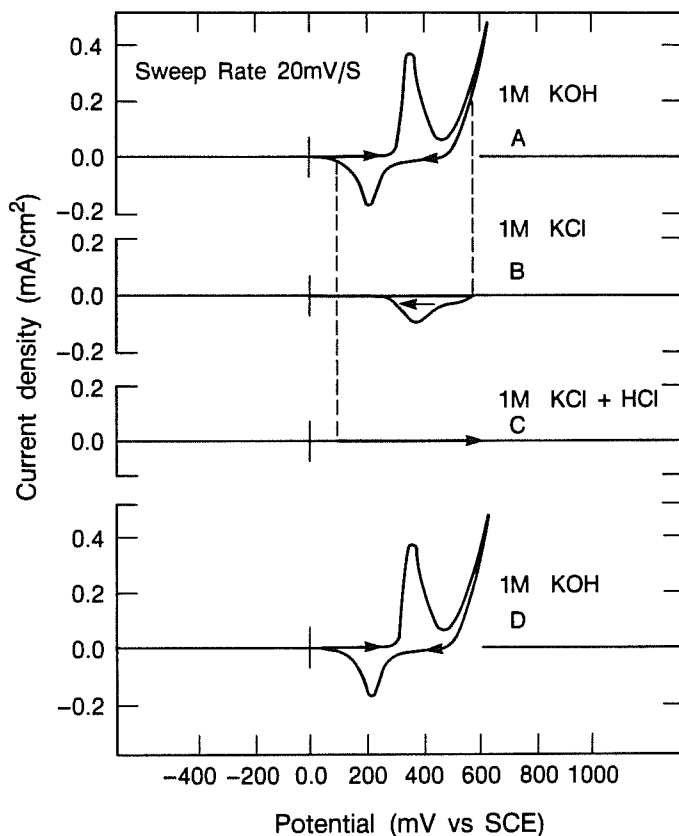


Fig. 9. Sequential cyclic voltammetry of a hydrated nickel oxide/SnO₂:F/glass electrode at a sweep rate of 20 mV/s, (A) 1.0M KOH, (B) 1.0M KCl, (C) 1.0M KCl+HCl and (D) 1.0M KOH

Lithium was added to the electrode by cycling in a saturated solution of LiOH, over the range of -500 to +700 mV (SCE), with a sweep rate of 20 mV/s. Changes in the initial voltammetry profiles for the lithiation of hydrated nickel oxide are shown in Fig. 10. As the electrode is cycled, both the height of the anodic current peak and the amount of the anodic charge decrease with the number of successive cycles, while the corresponding cathodic current peak remains substantially unaltered. Also, the overpotential of the oxygen gas evolution tends to increase during successive cycles. Another beneficial effect of the lithium ions is it decreases the breadth of the oxidation and reduction peaks. The largest effect is seen for the cathodic current peak. This is expected to increase the switching speed from the colored to the bleached states.

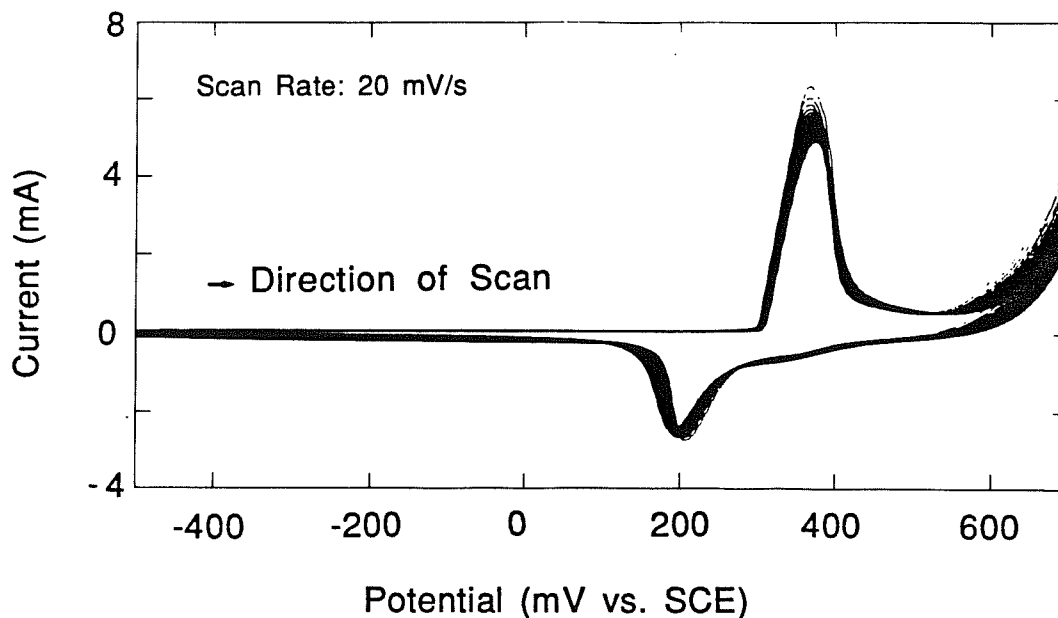


Fig. 10. Cyclic voltammeter of a hydrated nickel oxide/SnO₂:F/glass electrode in a saturated solution of LiOH, at a sweep rate of 20 mV/s.

4. CHEMICAL ANALYSIS

Several techniques were used to analyze the hydrated nickel oxide/SnO₂:F/glass electrodes. Both the chemical composition and the structure and morphology of the coating needed to be determined to help explain the nature of electrochromism in hydrated nickel oxide.

4.1 Ion Backscattering Spectrometry

Ion Backscattering Spectrometry (IBS) was performed on the hydrated nickel oxide film in the bleached state to determine the chemical composition and thickness^{6,21,22}. For the IBS analysis the Tandem accelerator spectrometer at Cornell University, Ithaca, NY, was used. The two samples examined were prepared under identical conditions. Also, for comparison the substrate was analyzed. In Fig. 11 is a backscattered spectrum of the hydrated nickel oxide film, showing good depth resolution and signal-to-noise ratio. The probe beam consisted of 2.14 MeV alpha particles at 60° from normal incidence to the sample in a vacuum of 5.3x10⁻⁴ Pa (4 x 10⁻⁶ torr). The elemental composition was oxygen, 0.78 MeV; chlorine, 0.93 MeV; nickel, 1.64 MeV; and tin, 1.88 MeV, in agreement with standard values²³. In addition, the compositions of the hydrated nickel oxide film and the conductive layer were determined²² to be NiO_{1.0} with a thickness of 12.5 nm and, Sn O_{1.9}: F, with a thickness of 0.440 μm (fluorine was determined by X-ray photoelectron spectroscopy). Also, chlorine was found as an impurity in these layers. Another IBS analysis used 3 MeV alpha particles incident at 7° from normal to the sample. The substrate was found to contain the elements oxygen, 1.07 MeV; and silicon, 1.69 MeV. The film, with the conductive layer and substrate, was composed of oxygen, 1.07 MeV; silicon, 1.56 MeV; chlorine, 1.89

MeV; nickel, 2.30 MeV; and tin, 2.69 MeV. The chlorine is an impurity in the tin oxide resulting from the deposition process. The data obtained correlated with standard tabulated values²³.

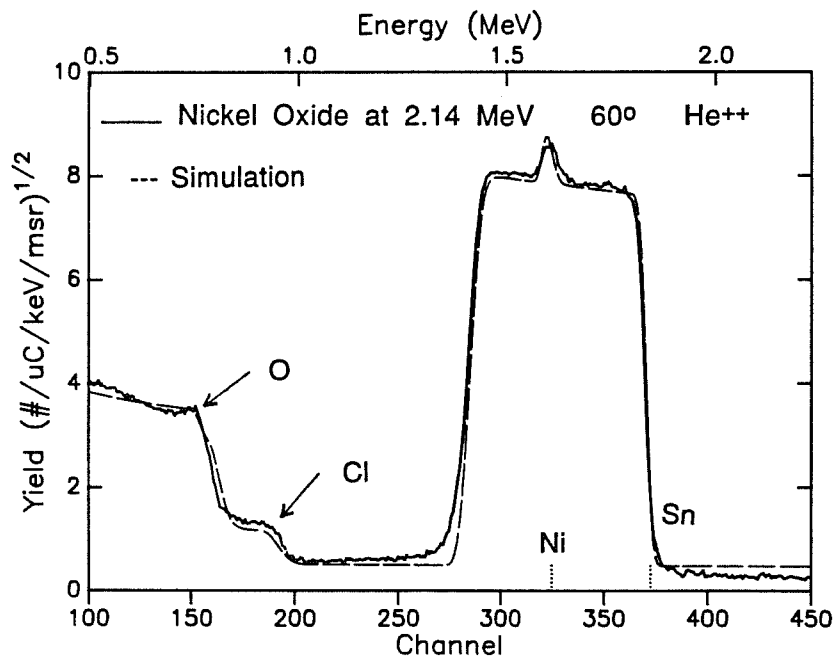


Fig. 11. Ion Backscattered spectrum of a hydrated nickel oxide/SnO₂:F/glass electrode. A computer simulated spectrum is shown in dashed lines.

4.2 Auger and X-Ray Photoelectron Spectroscopy

Chemical analysis of the electrode was determined by Auger spectroscopy and X-ray photoelectron spectroscopy (XPS)⁶ (also known as ESCA). The Auger measurements were performed on a model 590 PHI scanning Auger microprobe. The XPS measurements were made on a PHI model 548 XPS spectrometer. Both Auger and XPS gave data consistent with that of backscattering spectrometry. An Auger depth profile is shown in Fig. 12. Near the surface is a highly oxidized region. Beneath the impurity region is a layer of nickel hydroxide followed by the interfacial region separating nickel hydroxide and tin oxide. A survey Auger scan after 15 seconds of sputtering is shown in Fig. 13. This survey details the nickel impurities to be chlorine, carbon, and nitrogen. Argon was implanted from the sputter beam.

To further probe the hydrated nickel oxide chemistry, XPS was employed. Comparative The XPS binding energies for nickel and oxygen for the hydrated nickel oxide layer are shown in Table 1. Our data compares well to known energies for NiO by other investigators²⁴⁻²⁸. In this study, the binding energy of the adventitious carbon-1s electron was noted at 284.7 eV. During calibration, adventitious carbon-1s peak occurred at 284.4 eV. The difference in energy is caused by charging of the sample. The shape and position of the nickel and oxygen peaks are shown respectively in Figs. 14 and 15. These results indicate that the state of the hydrated nickel oxide film is nickel oxide, at least under the ultra high vacuum condition of the XPS analysis. We have seen on occasion a double peak in the oxygen-1s, which could be interpreted as hydroxyl. In another XPS study on cycled anodically oxidized metal films and evaporated

nickel oxide films, different spectral peaks were found. These peaks were interpreted as $\text{Ni}(\text{OH})_2$ and Ni_2O_3 (Ref. 29).

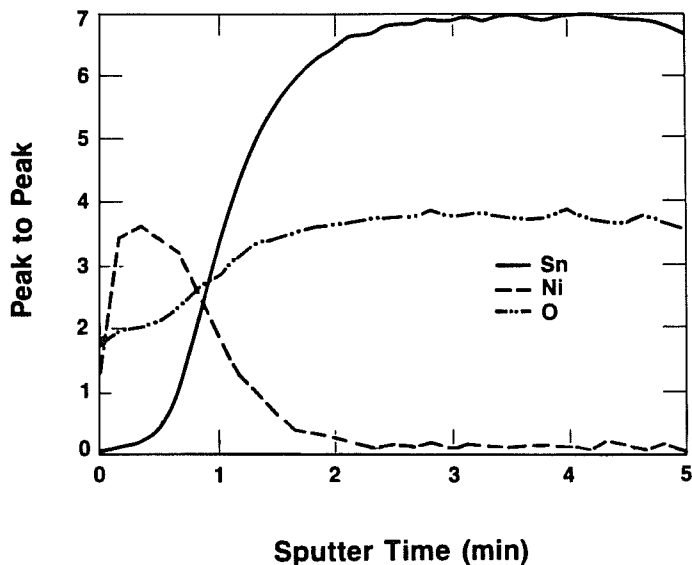


Fig. 12. Auger sputter depth profile of a hydrated nickel oxide/ SnO_2 :F/glass electrode showing its composition. The sputter rate is 40 nm/min for Ta_2O_5 .

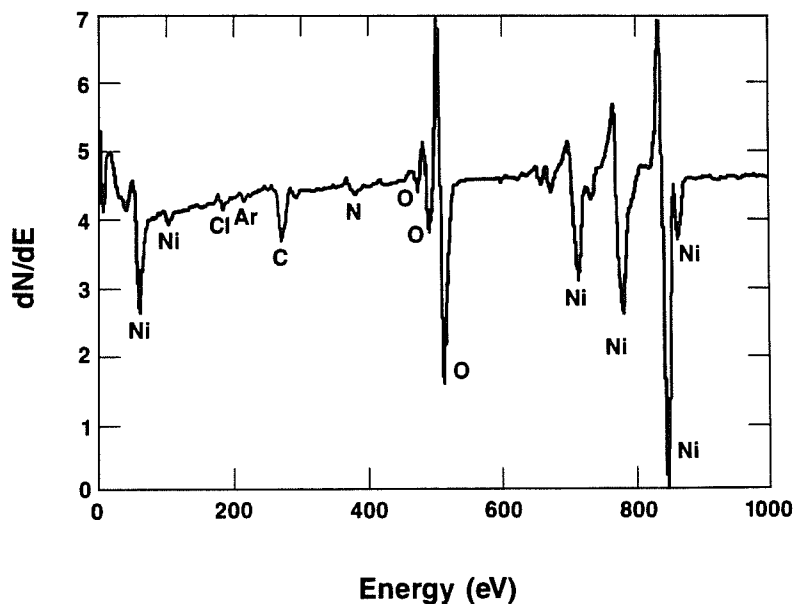


Fig. 13. Auger electron spectroscopy of a hydrated nickel oxide/ SnO_2 :F/glass electrode. This spectrum is taken after 15 seconds of sputtering. The sputter rate is 100 nm/min for Ta_2O_5 .

Table 1**XPS Binding Energies for Ni, NiO and Ni(OH)₂**
(All values in eV)*

Material	Ni-2p _{3/2}	Satellite	Ni-2p _{1/2}	Satellite	O-1s	Ref.
This study	854.7	860.7	872.7	878.7	530.5	--
NiO	854.3	861.5	--	--	529.7	24
NiO	854.4	--	--	--	529.5	25
NiO	855.0	861.1	873.0	879.8	--	26
Ni(OH) ₂	856.4	862.2	--	--	531.5	24
Ni(OH) ₂	855.7	--	--	--	531.2	27
Ni	852.3	--	--	869.7	--	28

*All data adjusted for charging and differences in calibration.

4.3 In-situ Fourier Transform Infrared Spectroscopy

To gain a better understanding as to how electrochromic hydrated nickel oxide changes chemically in both colored and bleached conditions, in-situ spectroscopic techniques were utilized⁸. Chemical identification of molecular vibrations of hydrated nickel oxide was achieved by Fourier-Transform Infrared Spectroscopy (FTIR). An IBM-98 FTIR spectrometer with a custom in-situ electrochemical cell were used in this study.

After deposition, the film was rinsed in distilled water. Then the electrode was placed in a cell containing a 1.0M KOH (pH=13.8 at 22 C) electrolyte, where the cell was purged with nitrogen under a vacuum of 1.33×10^{-1} Pa (1×10^{-3} torr). The cyclic potential range was set from -500 to +700 mV at a scan rate of 50 mV/s. The spectra of the near and middle-infrared regions in both the bleached and colored states as seen in Fig. 16 show vibrational stretches of surface hydroxyl groups of nickel hydroxide and fundamental water and carbon dioxide vibrations. A complete listing of the vibrational peaks is tabulated in some of our prior work⁸.

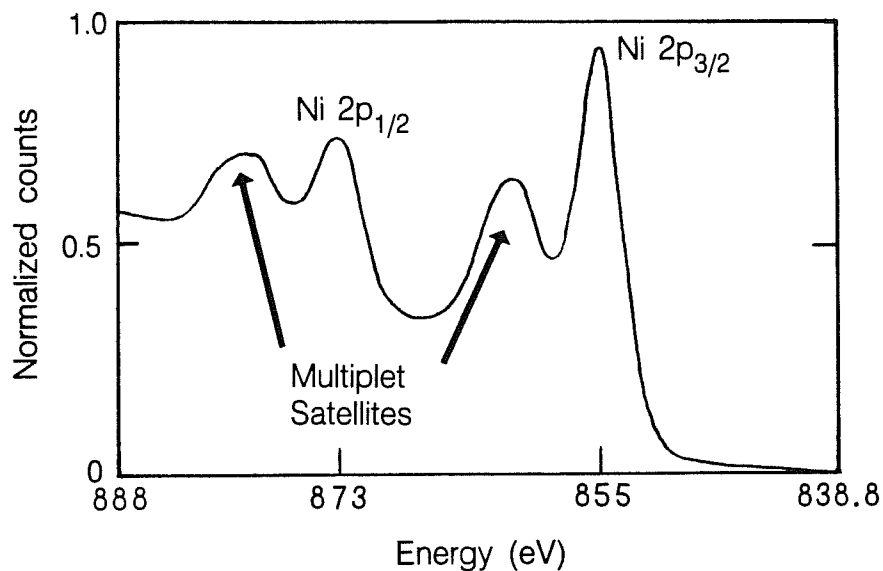


Fig. 14. X-ray photoelectron spectroscopy of the nickel-2p electrons in electrochromic hydrated nickel oxide, showing characteristic binding energies corresponding to NiO.

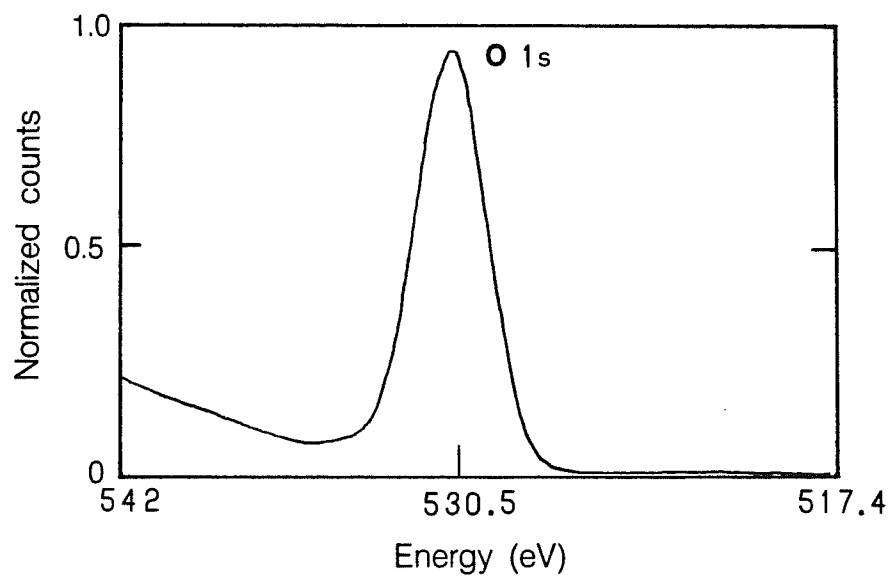


Fig. 15. X-ray photoelectron spectroscopy of the oxygen-1s electrons in electrochromic hydrated nickel oxide showing characteristic binding energies corresponding to NiO.

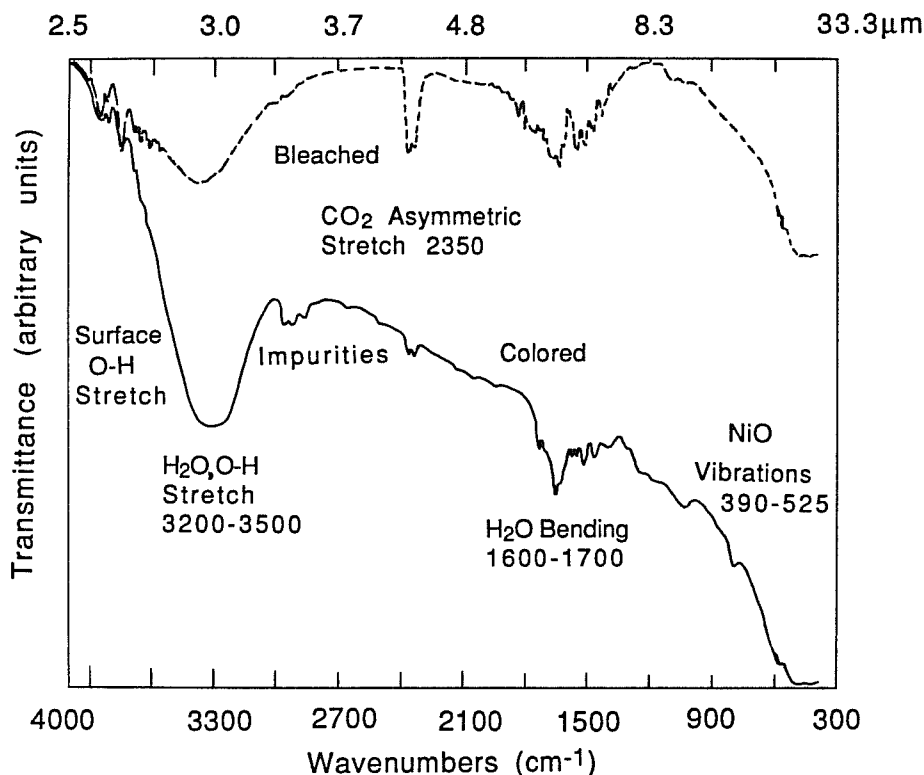


Fig. 16. In-situ FTIR spectra for electrochromic hydrated nickel oxide show characteristic molecular vibration regions. Both bleached and colored conditions are shown.

Infrared spectra of hydroxyl groups on the surface of hydrated nickel oxide generally consist of several absorption bands, with the wavenumber and relative intensity dependent on the type of hydroxide and degree of dehydroxylation³¹. Also, there are distinct types of surface hydroxyl groups in hydrated nickel oxide as a result of the different coordination bonding of oxygen atoms to nickel atoms. These groups are evident in Fig. 16 for both the bleached and colored modes in the wavenumber regions between 3600-3800 cm⁻¹. The location of the experimental vibrational stretches are in agreement with those noted by other investigators, but the peak- by-peak identification of each stretch is dependent on sample preparation and test conditions³⁰⁻³⁹.

Fundamental water vibrations are noted in Fig. 16 in the wavenumber regions of 3200-3500 cm⁻¹ and 1600-1700 cm⁻¹. Thus, both spectra indicate lattice water as a part of the nickel oxide's structure in its bleached and colored states, i.e., water molecules trapped in the crystal lattice by weak coordinate-covalent bonds to the nickel ions³². Other investigators have noted that the broad band having a center at 3450 cm⁻¹ and absorption at 1620 cm⁻¹ can be attributed to the stretching mode and the bending mode of the lattice water, respectively^{35-38,40}. Fundamental CO₂ vibrations (C-O asymmetrical stretch at 2350 cm⁻¹) are also evident in both conditions (Ref 39,41). The symmetric stretching vibration of CO₂ is inactive in the infrared because there is no change in the dipole of the molecule⁴¹. The nickel-oxygen vibration region occurring between 390-525 cm⁻¹ is shown in Fig. 17 for the bleached and colored modes.

Identification of the bleached state shows a broad vibrational stretch occurring in the wavenumber region of 400-510 cm^{-1} , with the central band at 430 cm^{-1} and shoulder at 483 cm^{-1} . Comparison of this stretch to those in the literature does show a correlation^{30,32,35-39,42,43}. The 430 cm^{-1} absorption may be the Ni-OH bending vibration for $\text{Ni}(\text{OH})_2$ and 483 cm^{-1} may be the hydroxyl group bending vibration, but the assignment of our experimental stretch is lower than those reported by others at 500-550 cm^{-1} (Ref. 30-32,34-39).

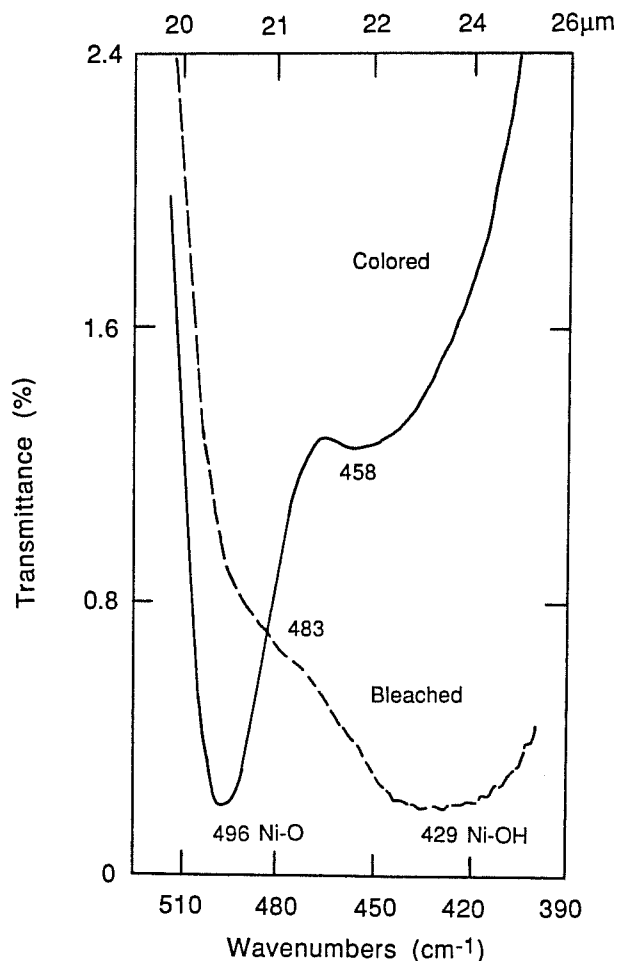


Fig. 17. In-situ FTIR spectra for electrochromic hydrated nickel oxide in the Ni-O vibration region. Both bleached and colored conditions are shown.

This difference in the vibrational stretch could be caused by differences in preparation and cycling parameters. These can affect the rate of charge injected or ejected into the electrode, which as a result causes shifts in the vibrational stretches in the infrared spectrum³². For the colored state, vibrational stretches again occur in the same wavenumber region of 400-510 cm^{-1} , with a band at 496 and shoulder at 458 cm^{-1} . They are also in agreement with vibrations reported by others^{30,33,38,42,43}. At 496 cm^{-1} the Ni-O vibration can be identified for NiOOH ⁴². From these experiments, it is clear that the molecular analysis of hydrated nickel oxide by FTIR is very complex. These in-situ experiments verify the presence of hydroxide phases on at least on the surface of the nickel oxide film. Supplemental work with angle-

resolved FTIR spectroelectrochemistry has confirmed a layer structure for hydrated nickel oxide on metallic nickel.³⁰ A proposed layer structure resulted from their work. A schematic of this layer structure is shown in Fig. 18.

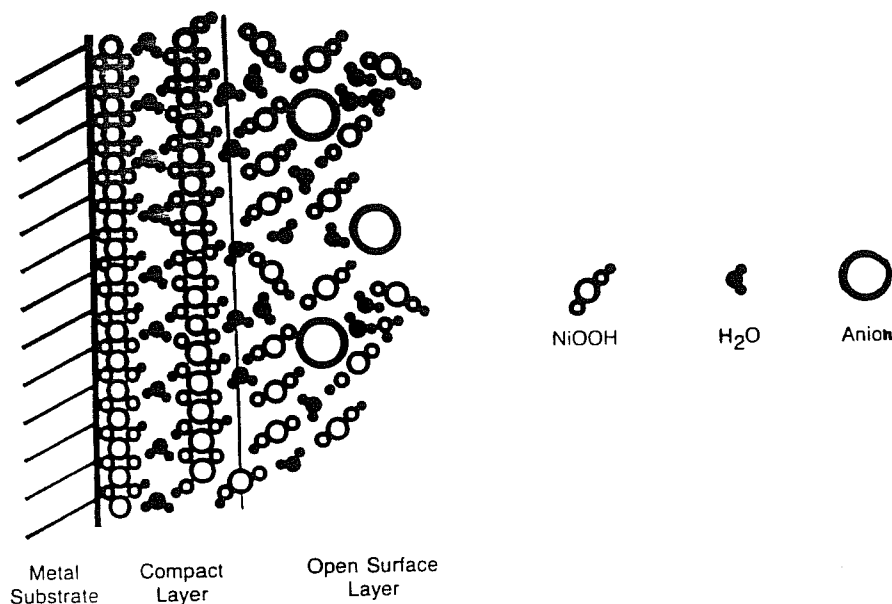


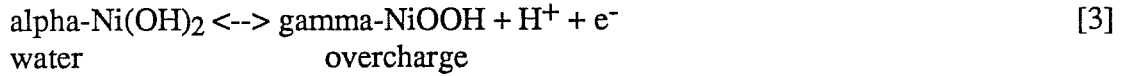
Fig. 18. Schematic diagram showing the structure of a hydrated nickel oxide film in the nickel oxyhydroxide phase (colored condition)(reproduced with permission, Ref. 30). Not shown to scale.

The results of angle-resolved infrared spectroelectrochemistry revealed that on the surface is an open layer of beta-Ni(OH)₂ and hydroxyl groups with free water, under which are a compact layer of alpha-Ni(OH)₂ and bound water layers. As the electrode is oxidized or switched to the colored state the film transforms to an open surface layer of beta-NiOOH with free water over a compact layer of gamma-NiOOH and bound water. As further studies are performed we expect to gain a better understanding of the nature of electrochromism and its relationship to the physical and chemical changes in hydrated nickel oxide.

4.5 Hydrated Nickel Oxide Switching Mechanism

There is considerable discussion about the coloration reaction in hydrated nickel oxide. Another important issue is identification of the type and nature of the absorption center that is responsible for the coloration of hydrated nickel oxide. There are at least 4 different interpretations of the coloration reaction for nickel oxide. The problems encountered with interpretation can be summed up as follows: (1) Many of the films are prepared by different techniques including d.c, r.f. sputtering, e-beam evaporation, anodic and cathodic electrodeposition, the basic structures and density of these films differ, the films can be crystalline, amorphous or mixed; (2) After films are cycled in hydroxyl containing electrolytes they may partly or totally convert to a hydroxide; (3) The films may have a layer structure; (4) the films may be sensitive or be modified by the analysis technique; (5) The in-situ and ex-situ properties of the films may be very

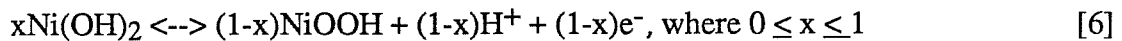
different; (6) the coloration reaction may be a surface and not a bulk phenomenon; (7) surface morphology, density and porosity greatly influence film properties. The classic reaction for the conversion and aging of crystalline hydrated nickel oxide battery electrodes is given as follows:^{13,14}



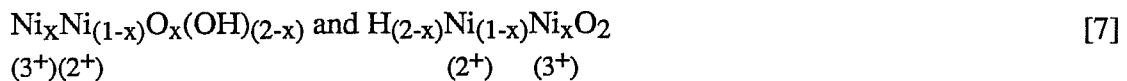
Much of our work on electrochromic hydrated nickel oxide and that of other researchers supports a simplified version of the former reaction^{4,6-8,44-46}.



In reality this reaction has some intermediate degree of completion following:



If we consider the redox state of the nickel then the two products become⁴⁷:



Reaction [3] follows a simple proton mechanism. Studies using nuclear reaction analysis (NRA) have supported the movement of protons during coloration and bleaching⁴⁴⁻⁴⁵. The nuclear reaction involved was 7 MeV $^{15}\text{N} + ^1\text{H} \rightarrow ^{12}\text{C}^* + ^4\text{He}$ and $^{12}\text{C}^* \rightarrow ^{12}\text{C} + 4.43 \text{ MeV}$ gamma radiation. The resulting radiation intensity is proportional to the hydrogen content in the film. The NRA work was done on samples, prepared by r.f. reactive sputtering from a nickel target, which had been electrochemically cycled. The estimated hydrogen level change was 2×10^{22} atoms/cm³ during about 50 mC/cm² charge extraction; in the bleached condition the hydrogen concentration was 1.2×10^{22} atoms/cm³. NRA has shown that electrochemically deposited films contain more hydrogen than films made by reactive e-beam evaporation. For samples made by reactive evaporation NRA analysis did not show significant change in the hydrogen level before and after coloration. These samples had coloration efficiencies (575 nm) of 32 cm²/C (Ref.45). In experimental devices of ITO/hydrated nickel oxide/Ta₂O₃/WO₃/Al, NRA has determined that the concentration of hydrogen in the nickel layer decreases during coloration while the hydrogen concentration increases in the tungsten oxide layer; no exchange of oxygen was noted²⁹. Also, our studies verified the importance of the presence of hydroxyl and its importance to coloration, although the proton appears to be the intercalated ion⁷. Regarding the bleached hydrated nickel oxide, our current work on anodic films using transmission electron microscopy (TEM) shows the only crystalline phase (very fine) to be cubic NiO, although an amorphous phase co-exists with this phase. Micrographs of this structure are shown in Fig 19. A Phillips 400 microscope operating at 100kV was used for this investigation. Other TEM studies on the microstructure of nickel oxide coating made by reactive r.f. sputtering from nickel target have shown cubic NiO with average grain size ranging from 7-17 nm. Some preferential orientation was noted for the (200) and (220) planes.

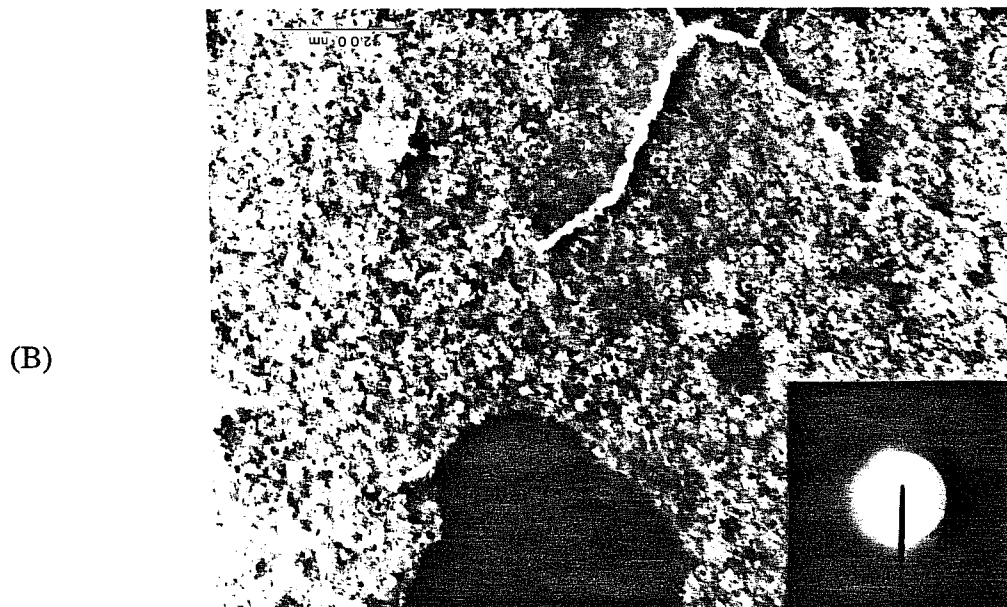
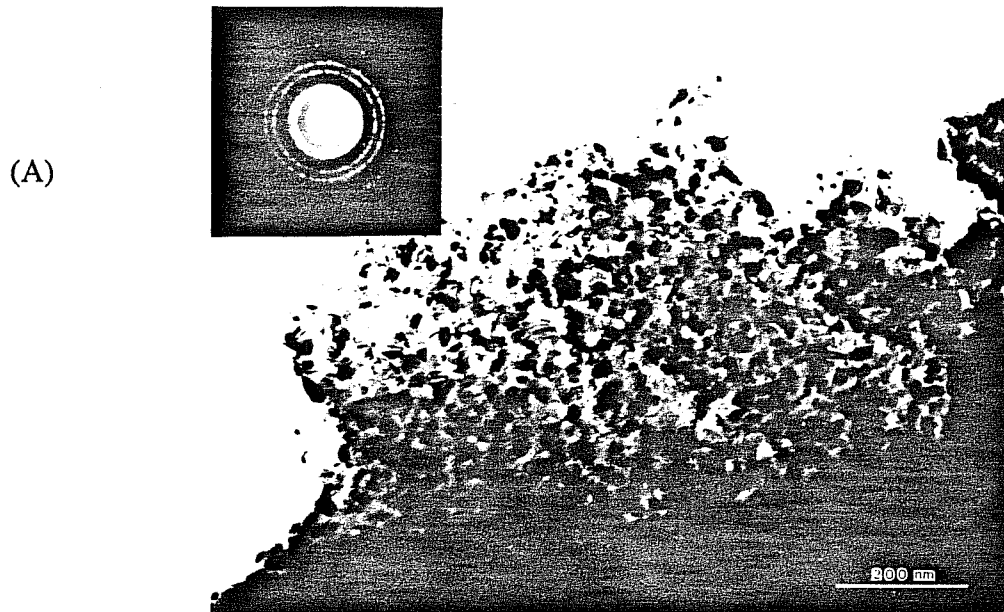


Fig.19. Transmission electron micrographs of electrochromic nickel oxide. Two bright field image shows a combination of small crystallites corresponding to cubic NiO coexisting with an amorphous phase. (A) Region showing large crystallites (B) Region showing amorphous character. This sample was made by anodic deposition.

This has been interpreted as grains with a fiber texture favoring the [001] direction⁴⁹. X-ray diffraction studies on films prepared by r.f sputtering of a NiO target have been performed³⁸. The result showed no diffraction peaks on film with approximate thickness below 0.6 μm . Thicker films with more sample heating revealed weak peaks corresponding to Ni_2O_3 which is probably hydrated in the form $\text{Ni}_2\text{O}_3 \cdot \text{H}_2\text{O}$ and can be rewritten as 2NiOOH . For thick films annealed at 300 and 500 C the transformation to cubic NiO was noted⁴⁹.

Other researchers support a purely hydroxyl reaction which originates also from studies on nickel battery electrodes following^{50,51}:



A correction to this reaction (and also to reaction [3]) has been shown where hydrated nickel oxide undergoes oxidation beyond the trivalent state to the quadravalent⁵²⁻⁵⁴, so the modification of reaction [8] would be:



where in this case, potassium from the KOH electrolyte is incorporated into the hydrated nickel oxide lattice. This result is quite important for the improvement of the charge/discharge characteristics of batteries.

Still another reaction has been proposed involving hydroxyl insertion into nickel oxide for films with low density⁵⁵:



Reaction [10] assumes hydroxyl ions are inserted into the nickel oxide and that the nickel oxide does not transform to $\text{Ni}(\text{OH})_2$. This reaction is based on results from optical multichannel analysis (OMA) and Raman spectroscopy^{55,56}. During OMA it is possible that water may be lost, so the reaction may be as follows⁵⁶:



Other FTIR and IBS studies give evidence that after cycling nickel oxide films convert to $\text{Ni}(\text{OH})_2$ (Ref 57). Obviously more work is need to verify the proper reaction and the determination of the role of both protons and hydroxyl ions. It is also important to separate out measurement artifacts from actual differences in samples. An investigation as to the structure of electrochromic hydrated nickel oxide may help us understand this better.

5. OPTICAL ANALYSIS

Hydrated nickel oxide films have been shown in the reduced form ($\text{Ni}(\text{OH})_2$) to be a p-type semiconductor with effective band gap of 3.6-3.9 eV, with significant tailing of states into the energy gap⁵¹. Also this form shows strong absorption in the UV region below 300 nm. The oxidized form behaves as an n-type semiconductor with a band gap of 1.7-1.8 eV, also with a tailing of states in the energy gap. This form shows strong broad absorption in the visible region and its absorption has been assigned to band to band transitions involving charge transfer from oxygen and higher valency nickel atoms⁵⁸. The tailing of states is typical of amorphous semiconductors. During the time in which both the oxidized and reduced states are present in the material transient photocurrent can be generated⁵¹. The complex dielectric function $\epsilon = \epsilon_1 + i\epsilon_2$, has been measured on sputtered electrochromic nickel oxide⁴⁶. It was determined that bleached hydrated nickel oxide has approximately $\epsilon = 4 + i0$ from 0.4-2.4 μm . fully colored (extraction of $5.7-6.5 \times 10^{21}$ electrons) ϵ varies from $\epsilon = 3.5 + i1.7$ at 0.4 μm to a peak with $\epsilon = 4.5 + i2$ at 0.8 μm to $\epsilon = 6 + i0.5$ at 2.4 μm .

5.1 Optical Spectroscopy

For optical measurements a hydrated nickel oxide electrode was cycled in-situ in a Perkin-Elmer Lambda 9 spectrophotometer. The electrode was cycled in 0.05 KOH (pH=12.8) using a triangle potential from -500 mV to 750 mV at 0.1 Hz and allowed to complete 5 cycles before spectral data was taken. The spectral data was obtained relative to an uncoated substrate in the same cell configuration. Integrating with respect to the solar (air mass 2), solar near-infrared and the photopic spectrum⁵⁹, the transmittances are $T_s(\text{bleached})=101\%$, $T_s(\text{colored})=54\%$, $T_{\text{nir}}(\text{bleached})=101\%$, $T_{\text{nir}}(\text{colored})=83\%$, $T_p(\text{bleached})=101\%$, and $T_p(\text{colored})=31\%$, respectively. The optical spectra of a hydrated nickel oxide electrode in its bleached and colored condition is shown in Fig. 20. The high transmittance values for the bleached condition are a result of the adsorption being low for the hydrated nickel oxide thin films. The antireflection effect caused by the hydrated nickel oxide layer on the surface causes an increase in the transmission over that of the uncoated substrate.

Other optical experiments performed involved time-transmittance measurements at different wavelengths⁸. An example of this data is shown in Figs. 21 and 22. The response for 420 nm at various scan rates (10, 20, 50, 100 mV/s) are shown. For coloration at slow scan rates (10, 20 mV/s) the slopes are much larger than those of both bleaching regions. One can physically observe coloring occurring faster than bleaching. For the faster scan rates (50, 100 mV/s), the same tendency is still apparent. One also notes that at these rates residual coloration is evident as the film changes in optical density. Some of our best films have been cycled 5×10^3 times from 80-22% transmittance at 525 nm without appreciable change in the optical properties, after 10^4 cycles we have observed some residual coloration, but after a rest period the film returned to its bleached condition. The film were cycled from -500 to 800 mV for 1500 cycles/day continuously.

Research with laser deflection has shown that stress changes are seen in hydrated nickel oxide films during switching¹⁶. It has been estimated that a tensile stress of the order of 10^8 N/m was developed in the film during coloration. The stress disappearing during bleaching. The stress is reversible. The cause of the stress change is probably related to the extraction of protons during coloration, and is typical of

intercalated materials. This effect probably occurs in other electrochromic films too, and may be responsible for mechanical changes in the film over time.

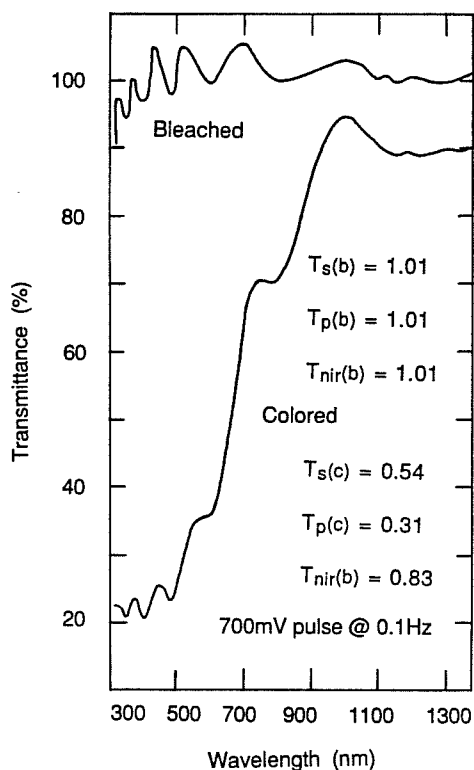


Fig. 20. Spectral transmittance of electrochromic nickel oxide/tin oxide/glass for the bleached and colored conditions. The data is taken relative to a tin oxide/glass substrate.

From the experiments performed in the time drive mode, Fig. 23 shows a plot of transmission (420 nm) versus applied voltage (20mV/s). This plot shows experimental and theoretical lines representing the coloration and bleaching sequences. To obtain 25% transmittance, complete coloration, the applied potential is 782 mV and for 85% transmittance, complete bleaching, the applied potential is -500 mV.

Fig. 24. depicts transmission versus total extracted charge for both the colored and bleached states. The total extracted charge to obtain a 25% transmittance coloring effect is approximately 300 mC and for a 85% transmittance bleaching effect is approximately -193 mC for an 8 cm² sample. The switching phenomena of hydrated nickel oxide involves first anodization (coloration) and then cathodization (bleaching). It is a solid state diffusion process where protons are being shuttled into and out of the NiO lattice. The hydroxyl ions also play an important role in this process³. By using a triangular potential, the complete coloration of the electrode to 25% transmittance takes 54 s at a scan rate of 20 mV/s. To obtain a

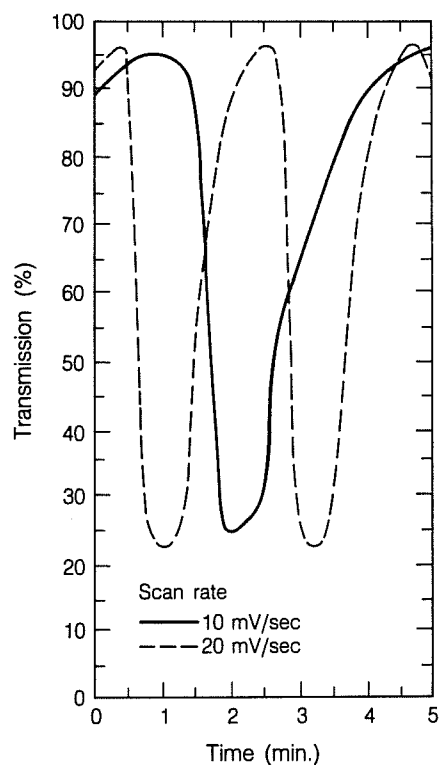


Fig. 21. In-situ dynamic transmittance at 420 nm of an electrochromic switching film. A triangular driving potential with 10 and 20 mV/s scan rates was used.

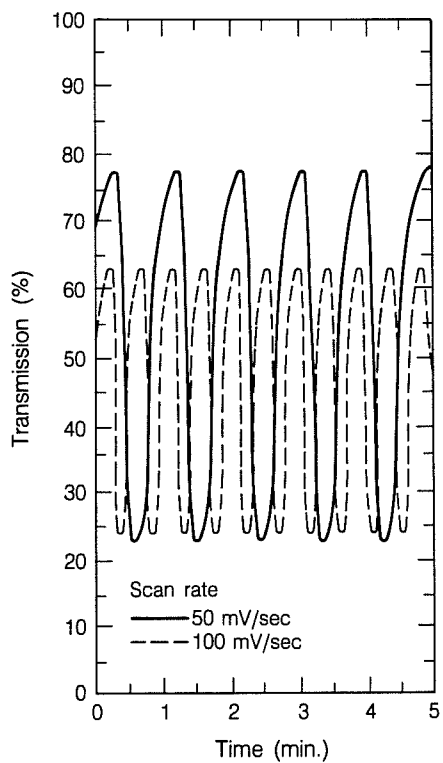


Fig. 22. In-situ dynamic transmittance at 420 nm of an electrochromic switching film. A triangular driving potential with 50 and 100 mV/s scan rates was used.

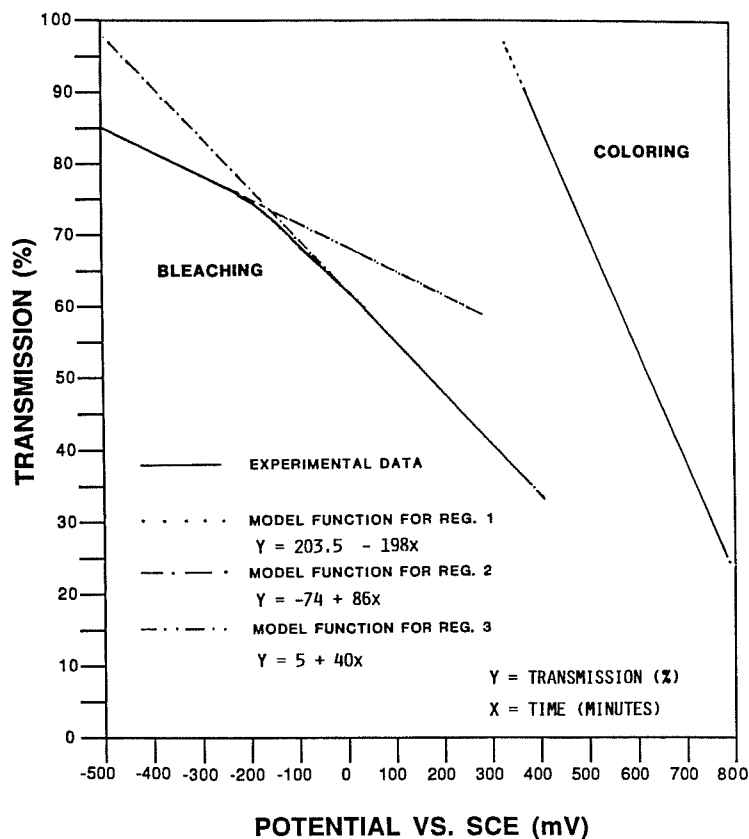


Fig. 23. Relationship between transmittance (420 nm) and applied voltage for both bleaching and coloring. Solid line shows actual data, dotted lines show linear regions.

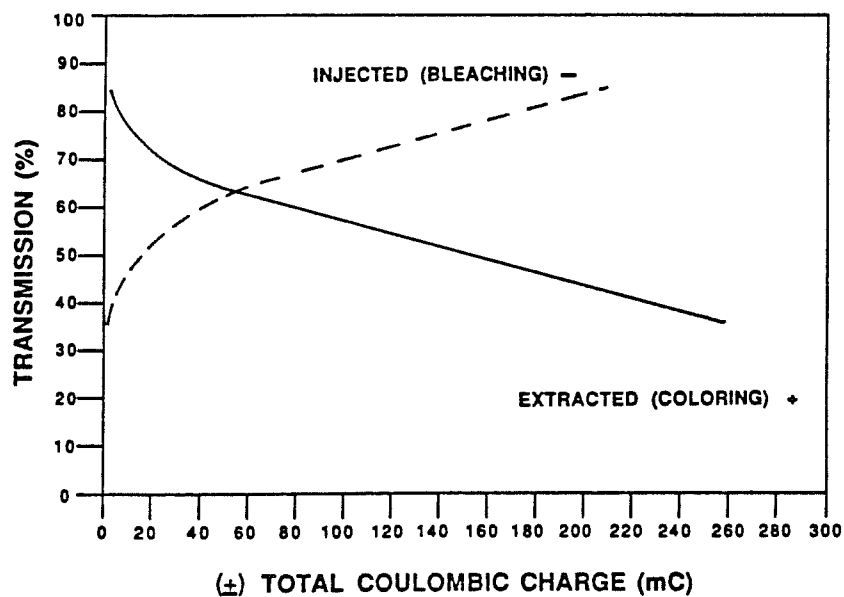


Fig. 24. Relationship between transmittance and injected/ejected charge. Data is for 420 nm and a 20 mV scan. Sample area is 8 cm².

45% transmittance value (in the bleached region) at the same scan rate, the time is 83 s. For a total bleaching effect, 85% transmittance, the time required is 120 s. It is important to note that the electrode response time is characteristically much shorter when using a d.c. potential source. Chronoamperometric studies (using a d.c. potential) have given a time constant of 1 s for chemically deposited films switching from 95-60% transmittance. For sputtered films a constant of 8 s has been determined for a 50-15% transmittance change¹⁶.

6. HYDRATED NICKEL OXIDE DEVICES

Using the electrode results, hydrated nickel oxide devices were constructed and evaluated. In these experiments the device structure was: glass/0.44 μm $\text{SnO}_2\text{:F}$ /120 nm hydrated nickel oxide/0.15 mm polymer electrolyte/0.44 μm $\text{SnO}_2\text{:F}$ /glass. These devices utilized polymeric quaternary ammonium hydroxide as the electrolyte which we developed⁴. The polymer electrolyte was synthesized from an quaternary ammonium chloride polymer by ion exchange between Cl^- and OH^- ions. The exchange was accomplished by using either an ion exchange resin or membrane dialysis. Fig. 25 shows the behavior of the voltammetry for two different devices. One of the devices has added lithium by electrochemical cycling in LiOH . The second device has hydrated nickel oxide that has been cycled in KOH .

Also, for these devices it is possible to draw the some conclusions about the greater peak sharpness obtained from the lithiated device. In both cases, the resin-hydroxylated polymer was used. The small cathodic peaks on the solid curve (610-640 nm) is probably caused by a chemical reaction with the silicone sealant. The a.c. impedance technique was used to measure the conductivity of the polymers. The conductivity of the resin-hydroxylated polymer was $8.03 \times 10^{-2} \text{ S cm}^{-1}$. The conductivity of the dialysis-hydroxylated polymer was $6.02 \times 10^{-2} \text{ S cm}^{-1}$. For comparison the conductivity of 1.0M KOH is $1.6 \times 10^{-1} \text{ S cm}^{-1}$.

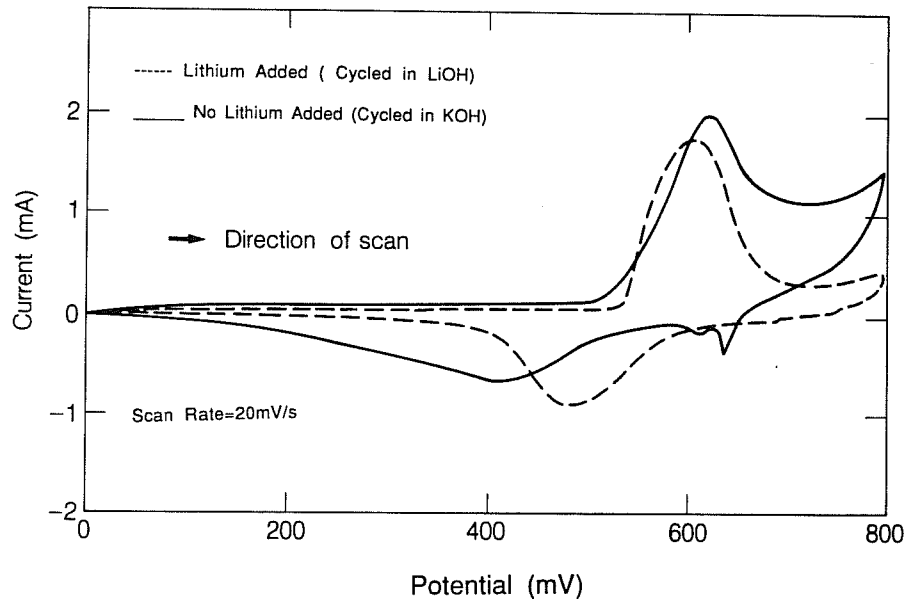


Fig. 25. Voltammetry of a nickel oxide device with a dialysis-hydroxylated polymer. The nickel oxide is shown with and without the addition of lithium. The scan rate was 20 mV/s.

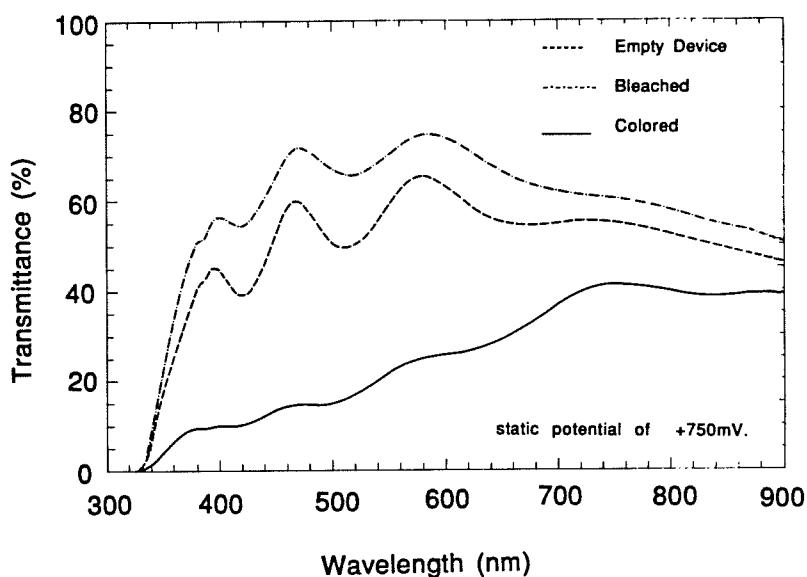


Fig. 26. Normal spectral transmittance of a nickel oxide electrochromic device, for the extended visible wavelength range (300-900 nm). The polymer was resin-hydroxylated. Data is shown for both bleached and colored states. The device was colored with a static potential of +750 mV. The transmittance of an empty device (no electrolyte) is provided for reference.

Normal transmittance measurements on the switching devices were performed over the visible and near-infrared wavelength regions. The device was colored using a static potential of +750 mV. The spectral transmittance (300-900 nm) of a hydrated nickel oxide device is shown in Fig. 26. The data shows the response from a device with the resin-hydroxylated polymer in its bleached and colored states. The interference peak in the visible region is reduced by filling the cell with the polymer, causing a change in the interfacial index of refraction. The antireflection effect produced by the polymer/hydrated nickel oxide interface results in higher transmission compared to the empty device. The maximum difference in transmittance between the bleached and the colored state occurs at a wavelength of about 500 nm.

The normal spectral transmittance (300-2000 nm) for the same sample showing the colored and bleached states is depicted in Fig. 26. The photopic transmittances (T_p) and the solar transmittance (T_s) (air mass 2) of this device are: $T_p(\text{bleached})=70\%$, $T_p(\text{colored})=23\%$ and $T_s(\text{bleached})=50\%$, $T_s(\text{colored})=23\%$. For comparison an empty device had optical properties of $T_s(\text{empty})=44\%$ and $T_p(\text{empty})=57\%$.

Hydrated nickel oxide devices were analyzed in the cyclic time mode at a wavelength of 500 nm. In this mode, the optical transmittance measurements are observed during switching of the film as a function of

time. The applied potential is stepped using a square waveform between two different values, with respect to the platinum reference electrode. To do this we used an Universal Programmer (EG&G, Princeton Applied Research, Model 175). This programmer permits one to switch the potential between two different levels, at various time intervals (10, 20, 50 and 100 seconds), using a square wave function of time.

We used dynamic cycling to analyze the effect of the bleaching potential magnitude on bleaching level. For each negative half cycle we incrementally changed its magnitude over the range from 0 to -1.5 Volts, at 20 second intervals. The positive coloration potential remains fixed at +750 mV. For this experiment the device was filled with the dialysis-hydroxylated polymer. Fig. 28 shows the behavior of this device. For a voltage less than -1.1 V the switching time rapidly increases, and the transmittance of the bleached state goes to a value of about 23% with a period of 20 seconds. A transmittance value of 67% was noted for an applied voltage of -1.5 V. Under the voltage stepping condition the operational life of the device is shortened. After some hundreds of cycles, the surface of the hydrated nickel oxide layer is no longer uniform.

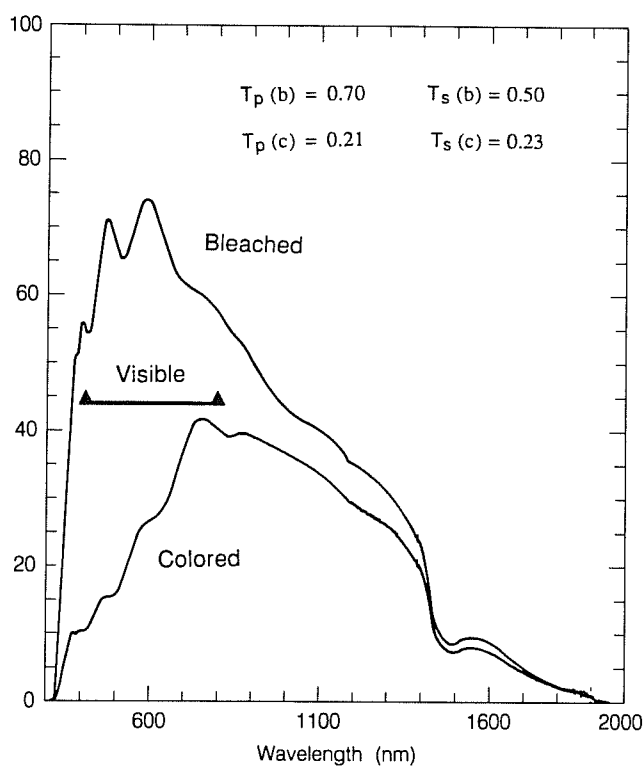


Fig. 27. Normal incidence solar spectral transmittance of the nickel oxide electrochromic device (the same device as in Fig. 26). Both the colored and the bleached states are shown.

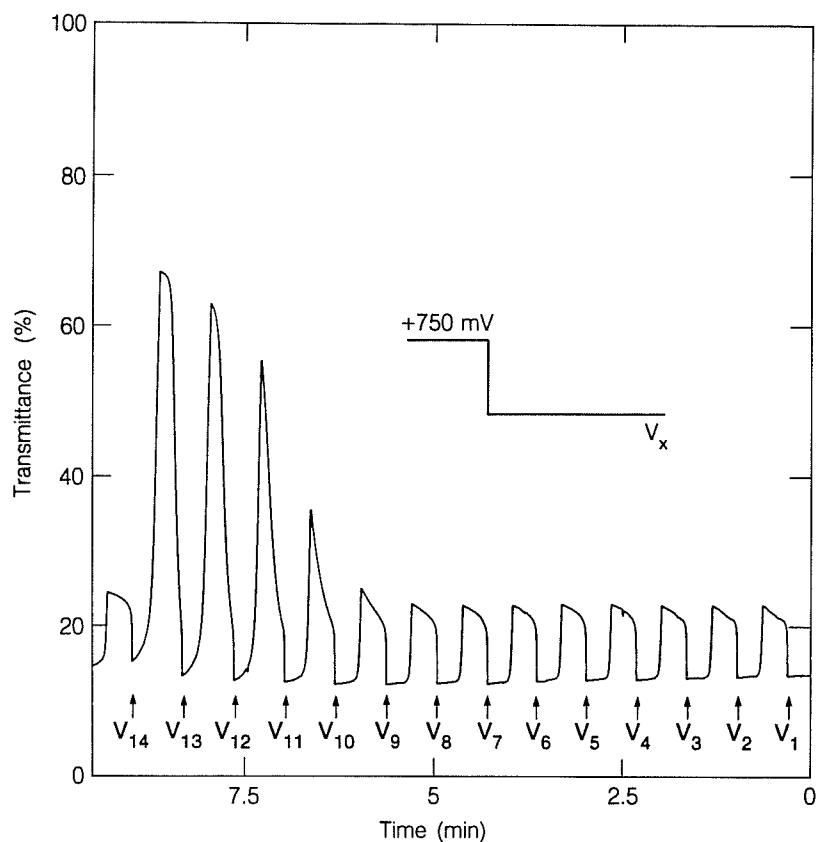


Fig. 28. Dynamic transmittance (500 nm) of a nickel oxide switching device using the dialysis-hydroxylated polymer electrolyte. For each step the magnitude of the negative potential half cycle is varied. The positive potential half cycle is fixed at +750 mV. (Note reversed time scale)

7. CONCLUSIONS

From the results obtained in these experiments, hydrated nickel oxide thin films exhibit favorable switching properties for application in architectural, automotive and aerospace glazings. In our studies, anodic deposition was used to deposit electrochromic hydrated nickel oxide onto doped tin oxide-coated glass in a nickel sulfate deposition bath. Also, other techniques can be used to deposit films.

The electrochemical properties of both the bleached and colored conditions were determined by cyclic voltammetry and NRA, indicating that the coloration reaction is $\text{Ni}(\text{OH})_2 \leftrightarrow \text{NiOOH} + \text{H}^+ + \text{e}^-$ with the proton as the dominant ion for coloration. Our in-situ FTIR analysis supports the formation of $\text{Ni}(\text{OH})_2$ and NiOOH . Other reactions involving different nickel oxide species and the hydroxyl ion as the dominant ion have been supported by studies of others. Our work indicates that the reversible process between bleached and colored states involves diffusion of the proton into the film, but the hydroxyl ion plays an important role in the reaction mechanism as verified from in-situ FTIR spectroscopy. Doping of hydrated nickel oxide with ions such as lithium improved the performance of the electrodes and devices. Doping can help increase the oxygen overpotential.

Ex-situ XPS has shown dehydrated films to have nickel binding energies close to NiO and oxygen binding energies between NiO and Ni(OH)₂. Ion backscattering and transmission electron microscopy experiments determined the chemical composition of the nickel oxide film in the dehydrated state to be NiO_{1.0}. The film is a combination of cubic NiO crystallites and amorphous regions. There is evidence to show that nickel oxide will convert to the hydroxide phase during cycling, but less evidence has shown the reverse. There is still a question as to the effect of defects (oxygen or nickel vacancies) have on the film optical properties.

Optical transmission studies on 120 nm hydrated nickel oxide film, gave a change in photopic transmission $\Delta T_p=70\%$. and solar response $\Delta T_s=47\%$ and near-infrared response $\Delta T_{nir}=18\%$. Transmission-time measurements indicated that there exists a linear relationship for both bleaching and coloring.

Electrochromic switching devices were summarized. The devices were constructed using hydrated nickel oxide as the switching material, a quaternary ammonium hydroxide polymer as the solid electrolyte, and fluorine-doped tin oxide for the electronic conductor layers. These devices show a modulation of the transmittance with the magnitude of applied voltage. Our best device to date (not yet optimized) showed the integrated photopic transmittance (T_p) to be $T_p(\text{bleached}) = 70\%$ and $T_p(\text{colored}) = 21\%$. The corresponding solar transmittance (T_s) was $T_s(\text{bleached}) = 50\%$, $T_s(\text{colored}) = 23\%$. A device without the polymer electrolyte had optical properties of $T_s(\text{empty}) = 44\%$ and $T_p(\text{empty})=57\%$. A further improvement is needed to perfect these devices.

There remain several challenges related to electrochromic hydrated nickel oxide. First, the electrochromic reaction for hydrated nickel oxide should be resolved. Only very simplified reactions have been reported. The significant coloration ions should be verified. There is considerable experimental evidence that the proton is responsible for coloration, however there is evidence the hydroxyl ion is important in the hydroxide to oxyhydroxide reaction. The amorphous and crystalline structure of the different types of electrochromic hydrated nickel oxide need to be better characterized. The surface morphology and porosity should also be determined because of their strong influence on coloration intensity and switching rate. With many of the analysis techniques there are questions about whether artifacts are introduced during analysis. The other large issue is that of comparison of samples made by different techniques; how similar or dissimilar are these samples? Also, there still remain the question whether other ions such as lithium in an aprotic environment will color hydrated nickel oxide effectively and reversibly? Also, beyond these issues there still lies the perfection of polymer electrolytes, ion storage layers and ion conductors for electrochromic hydrated nickel oxide devices.

ACKNOWLEDGEMENTS

I would like to thank all of my students and guest scientists who helped make this work possible. Also, I wish to thank Dr. G. Nazri (General Motors Research Laboratory, Warren, MI.) for his diligent efforts with the FTIR spectroscopic work. Also, I am grateful to Bruce Mayer (Watkins-Johnson, Scotts Valley, CA.) for supplying conductive glass and A. J. Yu (Cornell University, Ithaca, N.Y.) for his work on backscattering spectroscopy. Thanks are also due to Mr. D. Wruck and Dr. M. Rubin (LBL) and for use of the Lambda 9 Spectrophotometer. In addition, I wish to thank both Dr. A. Yee and Dr. S. Visco (LBL) for

their help on dialysis and a.c. impedance measurements. A special thanks goes to Mr. S. Selkowitz and Prof. J. Washburn (LBL) for their continued support of this project

This work was performed at the Lawrence Berkeley Laboratory, under a joint project between the Applied Science Division and the Materials and Chemical Science Division. The work was funded in part by the Assistant Secretary for Conservation and Renewable Energy, Office of Solar Heat Technologies, Solar Building Division of the U.S. Department of Energy under contract No. DE-AC03-76SF00098.

REFERENCES

1. C. M. Lampert, *Solar Energy Mater.* 11(1982)1.
2. J.L. Lagzdons, G.E. Bajars and A.R. Lysis, *Phys. Stat. Sol. (a)* 84(1984)K197.
3. N.R. Lynam and K.S. Koik, *Electrochromic Mirror*, U.S. Patent 4,712,879 (1987).
4. A. Pennisi and C.M. Lampert, *Proc. SPIE* 1016(1988)131.
5. D. A. Corrigan, and M.K. Carpenter, "Electrochromic nickel hydroxide films and the effects of foreign metal ions", this book.
6. C.M. Lampert, T.R. Omstead and P.C. Yu, *Solar Energy Mater.* 14(1986)161.
7. P.C. Yu, G. Nazri and C.M. Lampert, *Solar Energy Mater.* 16(1987)1.
8. P.C. Yu and C. M. Lampert, *Solar Energy Mater.* 18(1989) in press.
9. R.S. Schrebler-Guzman, J.R. Vilche and A.J. Arvice, *J. Appl. Electrochem.* 8(1978)67.
10. J.L. Weininger and M.W. Breiter *J. Electrochem. Soc.* 111(1964)707.
11. R.S. Schrebler-Guzman, J.R. Vilche and A.J. Arvia, *Corrosion Sci.* 18(1977) 765.
12. M. Fantini and A. Gorenstein, *Solar Energy Mater.* 16(1987)487.
13. P. Oliva, J. Leonardi, J.F. Laurent, C. Delmas, J.J. Braconnier, M. Figlarz, F. Fievet and A. DeGuibert, *J. Power Sources* 8(1982)229.
14. H. Bode, K. Dehmelt and J. Witte, *Electrochim Acta* 11(1966)1074.
15. D.M. MacArthur, *J. Electrochem. Soc.* 117(1970)422.
16. A. Gorenstein, F. Decker, M. Fantini and E. Estrada, "Hydrated nickel oxide films: electrochemical and related physical properties", this book.
17. D.M. MacArthur, *J. Electrochem. Soc.* 117(1970)729.

18. R. Barnard, C.F. Randell, and F.L. Tye, *J. Appl. Electrochem.* 11(1981)517.
19. J.L. Weininger, Proc. of the Symposium on The Nickel Electrode, R.G. Gunter, edit, *The Electrochem. Soc.* 82-4(1982)1.
20. O.G. Volynskii, and Y.N., Chernykh, *Sov. Electrochem.* 13(1978)1619
21. J. F. Ziegler, *New Uses of Ion Accelerators*, Plenum, New York, N.Y. (1975)
22. W.K. Chu, J.W. Mayer, and M.A. Nicolet, *Backscattering Spectrometry*. London, Academic Press, 1978.
23. L. Doolittle, *Nucl. Instrum. Methods.* B9(1985)344.
24. K.S. Kim, W.E. Baitinger, J.W. Amy, and N. Winograd, *J. Elect. Spect. Relat. Phenom.* 5(1974)351.
25. K.S. Kim, and R. E. Davis, *J. Elect. Spect. Relat. Phenom.* 1(1972/73)251.
26. L.J. Matienzo, L.I. Yin, S.D. Grim, and W.E. Swartz, Jr., *Inorg. Chem.* 12(1973)2762.
27. N.S. McIntyre, T.E. Rummery, M.G. Cook, and D. Owen, *Electrochem Soc.* 123(1976) 1164.
28. C. D. Wagner, W.M. Riggs, L.E. Davis and J.F. Moulder, "Handbook of X-ray Photoelectron Spectroscopy", PHI, Eden Prairie, MN, 1979.
29. K. Bange, F.G.K. Baucke, B. Metz, *Proc. SPIE* 1016(1988)170.
30. G. Nazri, D.A. Corrigan and S.P. Maheswari, *Langmuir* 5(1989)17.
31. A.A. Tsyganeko, and V.N. Filimonov, *Spectr. Lett.* 5(1972)477.
32. F.P. Kober, *J. Electrochem. Soc.* 112(1965)1064.
33. F.P. Kober, *J. Electrochem. Soc.* 114(1967)215.
34. N. Minkova, M. Krusteva and G. Nickolov, *J. Molec. Struct.* 115(1984)23.
35. S.M. Rakhovskaya, S.A. Egorova, N.E. Bolotina and R.E. Tugushev, *Kolloid. Zh.* (Translated) 47(1985)195.
36. I.K. Kuchkaeva, I.S. Shamina, P.N. Bityutshii and L.A. Chetovshaya, *Zh. Prikl. Spektrosk.* (Translated) 17-5(1972)921.
37. I.S. Shamina, S.M. Maladin O.G. Rakhovskaya and L.A. Vereshchagina, *Electrokh.* (Translated) 10(1974)1571.

38. J.F. Jakovitz, Proc. of the Symposium on The Nickel Electrode, R.G. Gunter, ed., The Electrochem. Soc. 82-4(1982)48.
39. M. Houalla, V. Perrichon and P. Turlier, Comp. Rend. Acad. Sc. Paris C284-1(1977)1.
40. P.J. Lucchesi, and W.A. Glassen, J. Electrochem. Soc. 78(1956)1347 .
41. R. Silverstein, G. Bassler, and T. Morrill, Spectroscopic Identification of Organic Compounds, Wiley, N.Y., 4th Ed.(1981), p. 96.
42. Sadtler Research Lab. Grating Spectra Inorganics Y 898K, Y 226S, Sadtler Research Laboratories Inc., Philadelphia, PA. (1965).
43. R.A. Nyquist, and R.O. Kagel, Infrared Spectra and Inorganic Compounds., Academic, Orlando, FL, (1971), p. 236.
44. J.S.E.M. Svensson and C.G. Granqvist, Proc. SPIE 653(1986)10.
45. J.S.E.M. Svensson and C.G. Granqvist, Appl. Phys. Lett. 49(1986)1566.
46. A. Pennisi and F. Simone, Proc. SPIE 1016(1988)176.
47. F. G. K. Baucke, "Reflectance Control of Automotive Mirrors" this book.
48. W. Estrada, A.M. Andersson and C.G. Granqvist, J. Appl. Phys. 60(1988)3678.
49. S. Yamada, T. Yoshioka, M. Miyashita, K. Urabe and M. Kitao Proc. SPIE 1016(1988)34.
50. M.K. Carpenter, R.S. Conell and D.A. Corrigan, Solar Energy Mater. 6 (1987)333.
51. M. K. Carpenter and D.A. Corrigan, J. Electrochem. Soc. 136(1989)1022.
52. J. Desilvestro, D.A. Corrigan and M.J. Weaver, J. Electrochem. Soc. 135(1988)885.
53. D.A. Corrigan and S.L. Knight, J. Electrochem. Soc. 136(1989)613.
54. J. Desilvestro, D.A. Corrigan and M.J. Weaver, J. Phys. Chem. 90(1986)6408.
55. P. Delichere, S. Joiret, A. Hugot-Le Goff, Proc. SPIE 1016(1988)165.
56. P. Falaras, A. Hugot Le Goff and S. Joiret, "Optical techniques for the study of electrochromic phenomena: application of Raman spectroscopy and optical multichannel analysis (OMA) to the coloration of oxides and polymer films", this book.
57. N.R. Lynam and H.R. Habibi, Proc. SPIE 1016(1988)63.

58. J.D. E. McIntyre and D.M. Kolb, Symp. Faraday Soc. 4(1970)99.
59. F.A. Barnes, ed. RCA Electro-Optics Handbook., RCA Corporation, Harrison, N. J. (1974).